Minerals Engineering 36–38 (2012) 21–30

Contents lists available at SciVerse ScienceDirect

Minerals Engineering

journal homepage: www.elsevier.com/locate/mineng

An acoustic technique for measurement of bubble solids mass loading: (b) Monitoring of Jameson cell flotation performance by passive acoustic emissions

Steven J. Spencer [a,c,*], Ryan Bruniges [a,c,1], Giffard Roberts [a,c], Vic Sharp [a,c], Alvaro Catanzano [a,c], Warren J. Bruckard [b,c], Kevin J. Davey [b,c], Wen Zhang [a,c]

[a] Lucas Heights Research Laboratory, CSIRO Process Science and Engineering, Locked Bag 2005 Kirrawee, New South Wales 2232, Australia
[b] Clayton Research Laboratory, CSIRO Process Science and Engineering, Box 312, Clayton South, Victoria 3169, Australia
[c] Minerals Down Under National Research Flagship, Australia

ARTICLE INFO

Article history:
Available online 3 March 2012

Keywords:
Coal
Flotation bubbles
Process instrumentation

ABSTRACT

A passive acoustic emission (AE) monitoring system has been developed and tested in Australian coal washeries. The system detects naturally occurring stress waves in the pulp and froth zones of a flotation unit, utilising volumetric (hydrophone) and surface (broadband accelerometer) sensing technologies. The analyser has been proof-of-concept trialled on a coal washery Jameson cell. AE signals associated with both hydrophones mounted near and accelerometers mounted on a downcomer are shown to be sensitive to cell process conditions including aeration, feed solids and reagent addition rates. Accelerometers mounted on a Jameson cell downcomer are shown to be particularly sensitive to aeration rate with AE signals containing features that can be interpreted in terms of Minnaert bubble resonance theory. The frequencies of peaks in the Fourier power spectra are in this case used to estimate dominant bubble size and solids loading inside the downcomer. Passive AE monitoring is a promising approach for flotation cell performance on-line monitoring.

1. Introduction

A variety of flotation devices are used in Australian washeries, usually being characterised as either jet, column or mechanically agitated. A commonly used and important flotation device in Australian washeries is the Jameson jet cell (J-cell). However, despite the common use of Jameson cells in Australian washeries (and metalliferous ore beneficiation plants) there is currently no effective on-line system for monitoring J-cell performance and providing inputs for process control and optimisation.

The central role of bubble characteristics in the operation of the flotation cell is well recognised and research has concentrated on ways to characterise bubble size and particle attachment in both the pulp and froth zones of flotation cells. Pulp bubble size and void fraction distributions are known to strongly influence process efficiency. Similarly the stability of the flotation froth strongly influences product selectivity and recovery. Existing flotation performance monitoring methods are sometimes based on machine vision approaches for characterisation of the froth surface or pulp bubble size distribution. These methods do provide some process related information but are not in themselves reliable on-line predictors of unit performance in an industrial context. Bubble sizers are commercially available for estimating the size and distribution of bubbles in flotation cells and can be used for air flux measurements and suspended solids collection. Electrical impedance spectroscopy is being investigated as a flotation process monitoring tool (Hu and Firth, 2010). Recently there has also been interest in passive sensing of natural acoustic emissions (AEs) in flotation cells (Vanegas and Holtham, 2010; Spencer et al., 2010).

A large variety of industrial processes passively emit AE which can be used to indirectly sense process state and/or equipment condition (Boyd and Varley, 2001). Surface vibration and low frequency AE sensors have been used to infer the process and wear state of a variety of mineral processing devices. These unit operations include dense medium cyclones (DMCs) (Spencer et al., 2006a; Bruniges et al., 2008), semi-autogenous (SAG/AG) grinding mills (Campbell et al., 2006; Spencer et al., 2006b) and hydrocyclones (Hou et al., 1998; Neese et al., 2006). CSIRO has developed an AE analyser for process monitoring of DMCs (Bruniges et al., 2008; Spencer et al., 2008).

There is a vast literature on the acoustic properties of bubbles (Leighton, 1994) and the analysis of passive AE from bubbles (Al-Masry et al., 2005; Manasseh and Ooi, 2009). In a flotation cell,

* Corresponding author at: Lucas Heights Research Laboratory, CSIRO Process Science and Engineering, Locked Bag 2005 Kirrawee, New South Wales 2232, Australia. Tel.: +61 2 9710 6741; fax: +61 2 9710 6789.
E-mail address: steven.spencer@csiro.au (S.J. Spencer).
[1] Present address: Global Acoustics Pty Ltd., 12/16 Huntingdale Drive, Thornton, New South Wales 2322, Australia.

0892-6875/$ - see front matter © 2012 Elsevier Ltd. All rights reserved.
doi:10.1016/j.mineng.2012.02.011

AE is generated by bubble formation (Boyd and Varley, 2001; Manasseh and Ooi, 2009) near sparger, agitator or in the case of a Jameson cell, a downcomer, by re-excitation of 'adult bubbles' in the turbulent flow of the pulp within the tank (Kolaini and Goumilevski, 1997) and by the bursting and coalescence of bubbles in the froth (Vanegas and Holtham, 2008).

In this paper, some results from Australian Coal Association Research Program (ACARP) project C17042 concerning Jameson cell passive AE monitoring are interpreted in terms of Minnaert resonance theory for bubbles with attached solids (Zhang et al., 2012). An AE monitoring trial was performed on a Jameson cell at an Australian coal washery. The sensitivity of AE characteristics to changes in process conditions and sensor location in the downcomer, riser pulp and froth zones are demonstrated. The possibility of AE estimation of both the dominant pulp bubble size and solids loading are demonstrated.

2. The passive AE signature of bubbles in slurry

There is a well-known inverse relationship between the AE frequency of a freely-oscillating bubble and the bubble size – the so-called Minnaert relationship (Leighton, 1994; Manasseh et al., 2001). The extended Minnaert relationship between the resonant oscillatory frequency f_0 of a bubble with a 'clean' surface (no attached solids), bubble equilibrium radius R_0 and surface tension σ, may be written as follows (Leighton, 1994):

$$f_0 = \frac{1}{2\pi R_0}\sqrt{\frac{3\gamma P_\infty}{\rho} + \frac{2\sigma(3\gamma - 1)}{\rho R_0}}. \quad (1)$$

Here γ is the ratio of specific heats for the gas, ρ is the liquid density and P_∞ is the background hydrostatic pressure of the liquid. In this paper a 5% by weight solids slurry with particle SG of 1.6 (representative of coal feed in a washery fines circuit) and a ~1.2 value for the ratio of the specific heats is considered. Surface tension is usually a second order effect and does not substantially alter the Minnaert frequency for air bubbles in water or slurry with diameters of order 10 μm or more ($\sigma \sim 72$ mN m^{-1}). However, this situation may be complicated by the use of reagents which can affect the surface tension of bubbles to varying extents (Kihm and Deignan, 1995). The resonance frequency as a function of bubble size and depth in pulp can be visualised with the following plot.

Clearly there is an enormous range in bubble resonance frequency for bubbles in the 100–1500 μm radius range, being inversely proportional to bubble radius. Fig. 1 indicates a range of ~2–42 kHz for bubble radius decreasing from 1500 to 100 μm,

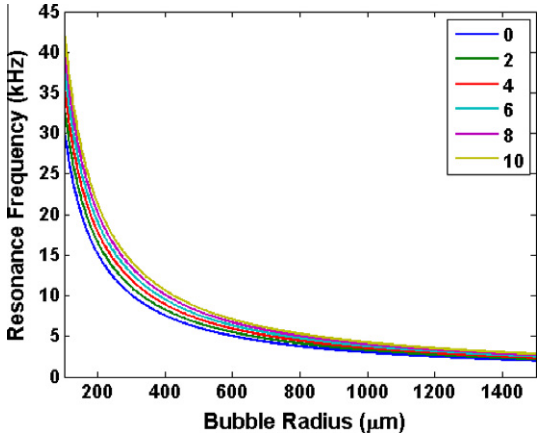

Fig. 1. Minnaert resonance frequency of a freely-oscillating bubble as a function of bubble radius (100–1500 μm) for different depths (m) in slurry.

which should cover the size range of bubbles likely to be generated in normal operation of Jameson cells and other flotation devices such as Microcel columns and mechanical cells. The resonance frequency for a given bubble radius does increase with depth in slurry (due to increased hydrostatic pressure) but this is a second order effect for tank depths of order 1–10 m (covering all likely tank depths from shallow Jameson cells to deep Microcel columns), in comparison with the variation with bubble size.

The Minnaert relationship can be modified to include surface mass loading representative of particle attachment. In this case the resonance frequency will decrease in comparison to an unloaded bubble due to the increased bubble wall mass loading, analogous to the effect of additional attached mass on the oscillation frequency of a spring. The opposite effect (resonance frequency increase with modulus of rigidity) has already been theoretically described in the case of a gas bubble with surface coating by a continuous, damped, elastic solid surface layer (Church, 1995). Mathematical models that describe simple harmonic motion of the bubble wall subject to the additional load of attached solids particles can be formulated based on an energy balance between slurry kinetic and gas internal energy under a variety of approximations (Zhang et al., 2012). The approach essentially extends the derivation of Leighton (1994) for the 'breathing' mode (spherically symmetric expansion and contraction) acoustic resonance frequency of an unloaded freely-oscillating bubble (Leighton, 1994) to include the effects of attached solids on the radiation mass of the bubble in the radius-force frame. One such model is a particular case for uniform solids coverage and is based on calculation of the total kinetic energy associated with bubble oscillation by integration of the differential kinetic energy in shells from the bubble wall across both a layer of attached solids of arbitrary thickness ε and to infinity in the external free slurry region. For attached solids particles of total mass M_S, it can be shown that the fundamental resonance frequency f_p of a solids loaded bubble is described in terms of the Minnaert frequency f_0 of an unloaded bubble of the same equilibrium radius by the following expression:

$$f_p = f_0\sqrt{\frac{1 + \varepsilon/R_0}{1 + \lambda\varepsilon/R_0}}. \quad (2)$$

Here the solids layer thickness is defined by:

$$\varepsilon \approx \frac{M_S}{4\pi\rho_{att}R_0^2\phi_S}, \quad (3)$$

and

$$\lambda = \frac{\rho_{att}}{\rho_{free}}, \quad (4)$$

is the ratio of attached (ρ_{att}) to free (ρ_{free}) slurry density. The parameter ϕ_S is the attached solids mass fraction. The attached solids mass fraction ϕ_S and volume fraction δ_S are related by $\delta_S\rho_S = \phi_S\rho_{att}$, where ρ_S is the solids density. A volume fraction of $\delta_S \approx 0.63 - 0.74$ is known to be reasonable for maximum close packing of near spherical particles in multiple layers.

Eq. (2) shows that as expected, the attachment of particles to a bubble surface, creating a layer of higher density than the surrounding slurry, decreases the fundamental resonance oscillation frequency of the bubble. It can be readily shown that Eq. (2) reverts to the standard Minnaert equation for $\varepsilon = 0$ and also for $\rho_{att} = \rho_{free}$ A re-arrangement of Eq. (2) allows the bubble solids loading associated with a spherically symmetric attached layer to be written as follows:

$$M_S = \frac{4\pi R_0^3\rho_{att}\phi_S[1 - f_r^2]}{[\lambda f_r^2 - 1]}. \quad (5)$$

Here $f_r = f_p/f_0$ is the ratio of solids loaded to unloaded resonance frequency.

A spherically symmetric, thin-layer of solids ($R_0 \gg \varepsilon$) is a useful first approximation in many flotation situations where strong particle hydrophobicity results in dominant bubble-particle adhesive over inter-particle cohesive forces (Omota et al., 2006). A 'thin-layer' approximation is also useful in dealing with the effects of particle attachment geometry on bubble acoustic resonance frequency. Although it is generally accepted that bubbles in the pulp phase of flotation systems are half-coated in particles (Ata and Jameson, 2005; Bournival and Ata, 2010), it can be shown that the angular disposition of attached solids in a 'thin-layer' on the bubble surface has only a higher order effect on the acoustic resonance frequency (Zhang et al., 2012).

Fig. 2 is a filled contour plot of attached solids mass loading as a function of the square of the ratio of loaded to unloaded resonance frequency (f_p/f_0) and bubble equilibrium radius. This plot was derived from Eq. (2) for a uniformly loaded bubble at 1 m depth and refers to coal slurry with particles modelled as monodisperse spheres of 50 μm diameter such that the attached particles are packed in a monolayer of $\delta_S = 0.6$ volume fraction, which is a reasonable upper limit on solids volume fraction in this situation (Omota et al., 2006).

A robust estimate of the maximum attached solids mass per bubble based on uniform coverage of a monolayer ('thin-layer') of monodisperse particles is as follows (Omota et al., 2006):

$$M_{S,\max} = 8\pi R_p^3 \rho_S \delta_S \left(1 + \frac{R_0}{R_p}\right)^2. \quad (6)$$

Here R_p is the particle radius. The maximum bubble solids loading at a given bubble size manifests in Fig. 2 as an upper limit in the bubble radius possible for a given ratio of loaded to unloaded resonance frequency. Fig. 2 (and Eq. (6)) shows that a maximum mass of ~0.01–1.4 mg of coal can be attached in a monolayer to the surface of a bubble of equilibrium radius $R_0 = 100$–1500 μm. For maximum solids loading there is a ~0.55–6.6% decline in acoustic resonance frequency over the $R_0 = 100$–1500 μm range of bubble equilibrium radius. As shown in Fig. 2, at any given solids loading there is a larger decline in resonance frequency for smaller bubbles. Basically it is easier to detect attached solids on smaller rather than larger bubbles. The minimum attached mass detection limit depends on the spectral resolution of the acoustic analyser instrumentation and the size of the bubble to which the solids are attached. For example, a 10 Hz spectral resolution corresponds to a minimum attached mass detection of $\sim 2 \times 10^{-5}$ – 1.2 mg for bubbles with equilibrium radius in the range $R_0 = 100$–1500 μm. The measurement of bubble passive AE fundamental resonance frequency in slurry could allow an estimate of attached solids loading, provided information was also available on unloaded bubble size.

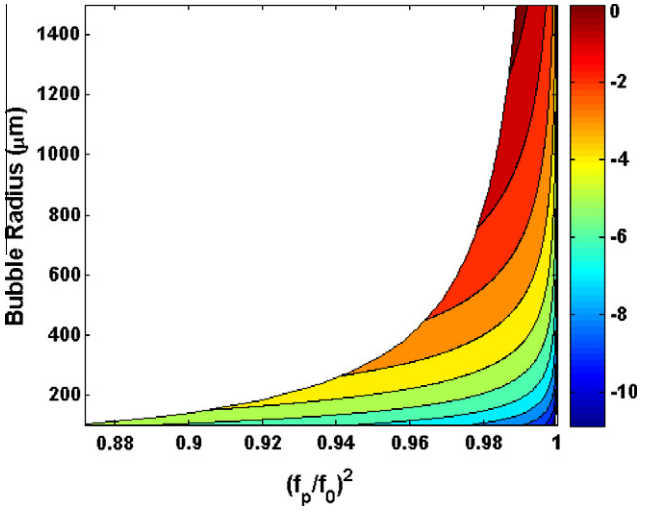

Fig. 2. Filled contour plot of natural logarithm of bubble attached solids mass loading (mg) as a function of the ratio of coal solids loaded to unloaded resonance frequency and bubble equilibrium radius.

It is interesting to estimate from this theory the resonance frequencies that might be associated with Jameson cell pulp bubbles observed in industrial flotation systems. The Jameson jet cell is thought to generate bubbles of typically ~300–500 μm diameter in the downcomer (Young et al., 2006). However, slightly larger bubble diameters of ~400–700 μm have been reported for a J300 cell and as large as ~1.2–1.7 mm averaged over a J5000 cell (Holtham and Power, 2002). Fig. 1 indicates that for ~300–700 μm diameter bubbles, as may be the likely size range created by a Jameson cell downcomer, the unloaded bubble Minnaert resonance frequency is ~9.2–21.5 kHz for a bubble subject to 1.5 m depth hydrostatic pressure. In comparison, for 1.0–2.0 mm diameter bubbles, as may be created by a Microcel sparger (Holtham and Power, 2002; Pyecha et al., 2006), the unloaded bubble Minnaert resonance frequency is ~3.6–6.75 kHz, for a bubble subject to 3 m depth hydrostatic pressure. Solids loading of oscillating bubbles will result in a lowering of individual bubble acoustic resonance frequency (see Eq. (2)). Variation in both the size of the bubbles and the amount of solids loading would at the least by superposition of individual bubble AE result in broadening of the apparent acoustic resonance frequency related to large numbers of bubbles. A passive AE monitoring system would need to be sensitive across a range of frequencies consistent with the resonance frequencies likely to be produced by both solids loaded and unloaded bubbles generated by that particular flotation device.

There are a number of difficulties in utilising the Minnaert relationship to estimate bubble size distributions in industrial flotation devices such as Jameson cells, including scattering, absorption, and group oscillation effects associated with bubble swarms that change the apparent resonance frequency (Manasseh and Ooi, 2009; Vanegas and Holtham, 2010). However, it may still be possible to derive meaningful estimates of bubble size if AE wave trains associated with individual bubbles can be identified by a signal windowing technique (Manasseh et al., 2001) or small numbers of bubbles are physically or acoustically isolated at a specific location in a cell. A key issue specific to passive AE monitoring is the rapid decay of emissions from any particular bubble soon after bubble formation (Leighton, 1994; Leighton et al., 1997), unless there is a continual injection of acoustic energy. This may limit the use of passive AE for estimation of bubble characteristics to regions near bubble formation (Manasseh et al., 2001) or where appropriate acoustic energy is continually provided. In the case of the Jameson cell, this issue suggests that passive AE monitoring of the downcomer region may be most fruitful. It should be noted that a number of possibilities for acoustic measurement of bubble characteristics based on active AE sensing have been reported that are relevant to pulp (Leighton et al., 1996,1997; Zhang et al., 2012) and froth (Vanegas and Holtham, 2010) regions.

3. The AE monitoring system

The Jameson cell AE data collected during the course of ACARP project C17042 and reported here was acquired using a modified form of the CSIRO AE analyser developed in previous ACARP project C16045 and described elsewhere (Bruniges et al., 2008; Spencer et al., 2008). The key components of the system are as follows:

- An IP66 rated industrial enclosure housing a custom-built four channel AE monitoring card and data logging computer. The system is suitable for long-term monitoring of separation and comminution devices in mineral processing plants and coal washeries.
- A 10–4 channel switching box which enables 10 AE sensors to be logged in consecutive groups of 4 by using the 4 channel CSIRO AE analyser.
- The use of hydrophones and accelerometers to sample volumetric and surface AE, respectively. Hydrophone signals are more directly representative of source AE characteristics in pulp and slurry. Accelerometer signals are very useful when the intrusive placement of a hydrophone within a region of particular interest (such as inside a Jameson cell downcomer) is problematic.
- Customised mounting assemblies for hydrophone AE monitoring of Jameson cells and Microcel columns.
- Steel and PVC accelerometer housings. PVC accelerometer housings are necessary in order to effectively monitor surface acoustics in plastic-lined tank walls or plastic downcomers in a Jameson cell. Surface acoustic contact was in this case achieved with silicon-based adhesive. For accelerometer contact AE monitoring of steel components, steel housings were used with mounting by bolts into welded M10 nuts.

The accelerometers used in this study were Endevco E7259B-10 broadband piezoelectric transducers. This type of accelerometers has previously been successfully used for monitoring dense medium cyclones in coal washeries (Spencer et al., 2008) and for monitoring flotation cells in the laboratory and coal washeries (Spencer et al., 2010) and is calibrated with a flat response up to ~50 kHz. The hydrophones used in this study were Bruel and Kjaer type 8103 calibrated to ~100 kHz. For both Jameson cell and Microcel column AE monitoring a total of four hydrophones and six accelerometers were utilised. Fig. 3 shows the hydrophone mounting rods (with hydrophones inserted) and PVC accelerometer housings used in the Jameson cell AE monitoring trial.

AE time series were acquired in the data gathering campaign. The subsequent post-processing characterised these results primarily in terms of total power and power spectra. An attempt is made to link features in the power spectra to bubble size and solids mass loading by Minnaert resonance theory.

4. Jameson cell

4.1. Plant configuration

The CSIRO AE analyser was installed on a J5000/16 (16 downcomer) Jameson cell in the fines circuit (two banks of two cells in series) at an Australian coal washery. A brief discussion of this proof-of-concept trial and some preliminary results for downcomer passive AE signature has been presented elsewhere (Spencer et al., 2010). Fig. 4 shows the relevant J-cell at the washery. This is a first stage primary cell in the two stage fines separation circuit. The PVC downcomers are ~300 mm external diameter and 5 m in length. The tank depth is approximately 1.5 m. A wash water tray was installed on the cell but was removed in the section in which the hydrophone rods were inserted and was not used during the time of the trial. The feed size was typically −300 μm with a top size of ~1.5 mm. The pulp density was run at ~4–12% with a solids ash content of ~4–12%. Baseline operating conditions were plant total (two modules) solids feed rate ~1600 th^{-1}, J-cell air feed rate ~800 $m^3\ h^{-1}$, frother addition rate ~10 $l\ h^{-1}$ and collector addition rate ~240 $l\ h^{-1}$. During much of the trial (subsequent to aeration variation tests) only one of the feed modules was in operation and hence the total plant feed rate was typically ~800 th^{-1}, with ~600 $m^3\ h^{-1}$ baseline aeration rate for each primary J-cell.

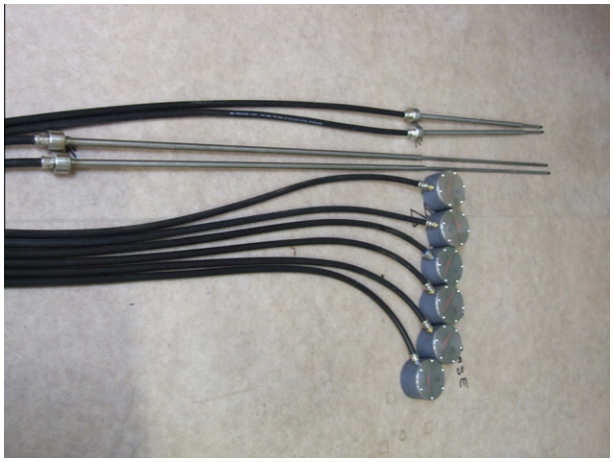

Fig. 3. Hydrophone mounting rods and PVC accelerometer housings used for the Jameson cell passive AE monitoring trial.

4.2. Experimental

A total of ten AE sensors were installed on the Jameson cell for the trial. Fig. 5 shows the sensor configuration near the selected downcomer for the conditional experimental program (the locations of hydrophones 2 and 4 near the tank wall and accelerometers 5 and 6 mounted on the inside of the tank wall are not shown here). An attempt was made to sense volumetric AE with hydrophones in both the froth (sensors 1 and 2) and pulp (sensors 3 and 4) at radial positions near a selected downcomer and near the adjacent tank wall. Four accelerometers (sensors 7–10) were placed at 1 m intervals from the nozzle of the same downcomer. The large number of sensors was utilised in order to gain some idea of the best location(s) to acoustically detect changes in process conditions and performance.

Fig. 6 is a photograph of the configuration of hydrophones plus some of the accelerometer mounting assemblies on the downcomer and the inside of the tank walls. In this trial the hydrophones were coated with a protective plastic layer to avoid potential abrasion from the slurry flow.

Fig. 4. Jameson cell (J5000/16) at an Australian coal washery.

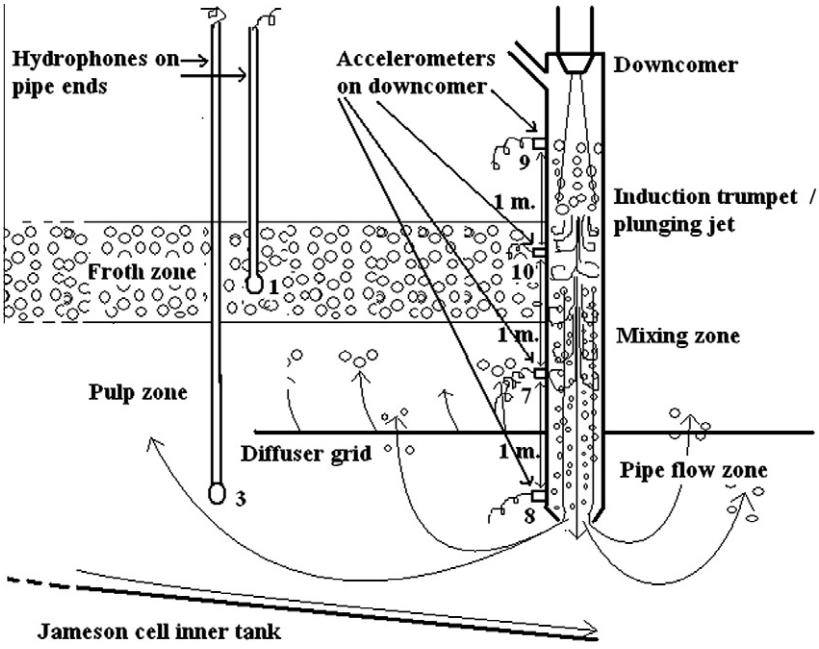

Fig. 5. Schematic diagram of sensor configuration near the selected downcomer during the Jameson cell AE monitoring trial.

Fig. 6. Photograph of sensor location for the Jameson cell AE monitoring trial. Perforated diffuser plate above downcomer discharge orifice shown.

A conditional experimental program was conducted on the coal washery Jameson cell as follows.

- Aeration rate was varied from 200 to 1200 $m^3 h^{-1}$ in 200 $m^3 h^{-1}$ steps.
- Frother addition rate was varied from 5 to 10 $l h^{-1}$ in 2 $l h^{-1}$ steps.
- Collector addition rate was varied from 150 to 240 $l h^{-1}$ in 30 $l h^{-1}$ steps.

The effect of turning off the feed valve to the individual downcomer was also investigated over the course of the trial. AE was also recorded for changes in plant feed rate during the trial.

4.3. Results

4.3.1. Example AE signatures

Figs. 7 and 8 show example AE time series at near baseline conditions for sensors S1 and S3 (hydrophones in froth and pulp near the downcomer, respectively) and sensors S8 and S9 (accelerometers mounted near the downcomer discharge orifice and 3 m upwards, respectively). There is clearly a discernible signature at all monitoring locations. Over a 10 s period the envelopes are reasonably steady and although similar in magnitude, the downcomer accelerometer AE signals appear to have significantly stronger high frequency components.

4.3.2. Air addition rate

Figs. 9 and 10 show the AE total power and power spectral density (PSD) for sensor 8 (the accelerometer nearest the discharge nozzle of the downcomer) as a function of cell total downcomer aeration rate. Fig. 9 shows that the AE spectra for the accelerometer mounted at the end of the downcomer are generally highly repeatable and the total power monotonically increases with aeration rate up to ~1000 $m^3 h^{-1}$ then decreases slightly. Only one power spectrum is shown in Fig. 10 for each aeration rate because of the high repeatability. For comparison, the AE spectrum associated with a closed downcomer valve (no slurry or air feed) is also shown. There is clearly a very strong effect of increasing AE response at most frequencies with aeration rate. This may be explained by the generation of additional bubbles within the downcomer as the aeration rate is increased, leading to an increase in the number of oscillating bubbles having contact (or near proximity) with the inside of the downcomer walls. The acoustic energy from the oscillating bubbles is transmitted through the downcomer wall to the acoustic sensors. The decrease in AE energy at the highest air rate may be a saturation effect as additional bubble loading begins to absorb more acoustic energy than it generates. These spectral features could also partially be the result of more vigorous and increased numbers of particle and bubble impacts on the inside of the downcomer wall due to an increase in the energy of the turbulent flow associated with higher aeration rates.

There are clearly strong spectral features in Fig. 10 at ~3, 5, and 9–12 kHz. In terms of the Minnaert relationship for unloaded single bubbles at ~1.5 m depth in slurry (see Fig. 1), these AE spectral peaks could represent bubbles of ~2140, 1270, and 710–540 μm diameter, respectively. This interpretation relies on the downcomer accelerometer passive AE response being dominated by a

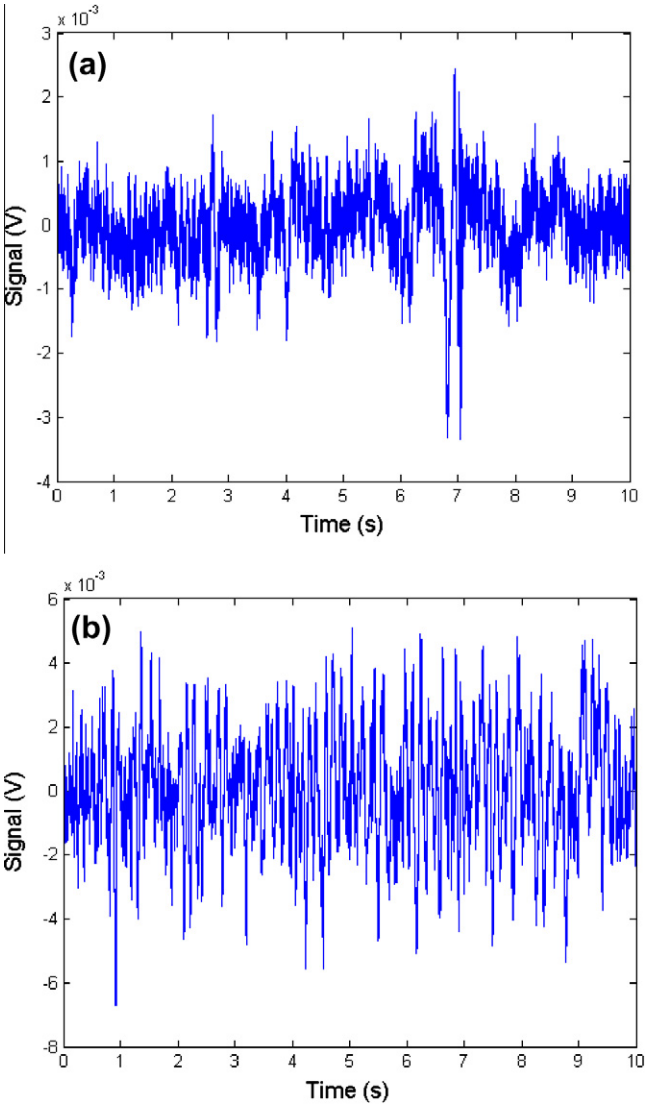

Fig. 7. Example AE time series (at near baseline conditions) for sensors: (a) S1 (hydrophone near downcomer in froth); (b) S3 (hydrophone in pulp near diffuser).

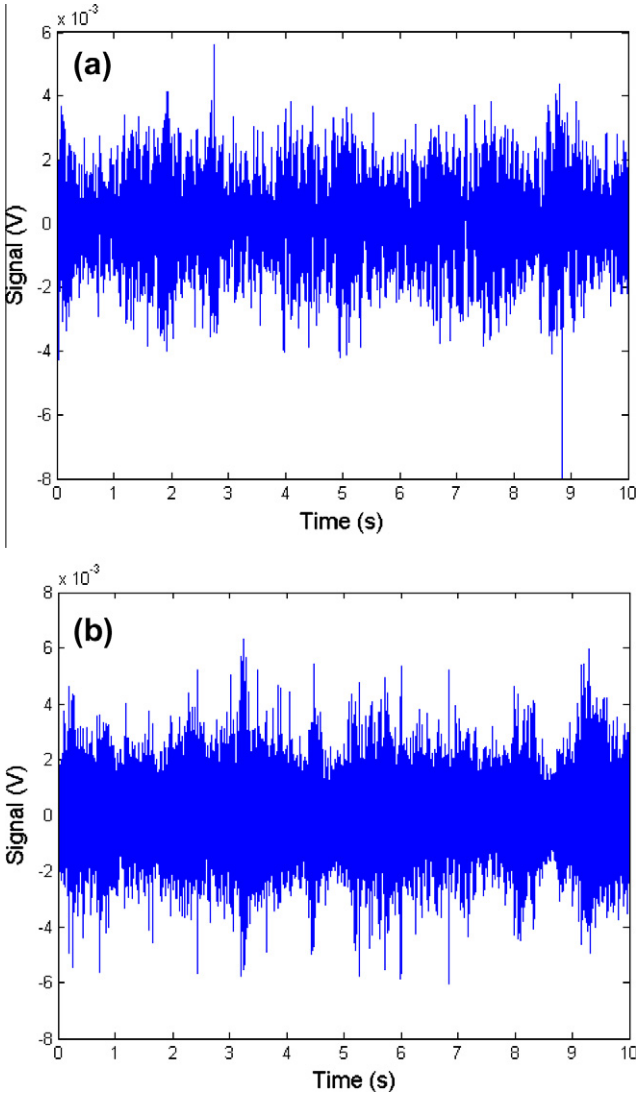

Fig. 8. Example AE time series (at near baseline conditions) for sensor: (a) S8 (accelerometer near downcomer discharge); (b) S9 (accelerometer 3 m above downcomer discharge).

superposition of individual bubble resonance and near resonance oscillation effects. Bubbles of ~710–540 μm diameter are at the upper end of the range that might be expected to be generated in a J-cell downcomer. There is a dominant low frequency (<2 kHz) component to the AE spectra which also increases with aeration rate. This is clearly also related to the addition of air and probably represents a combination of modal vibrations of the downcomer as a whole and collective pulsations of bubbles within the downcomer. As the aeration rate increases the relative importance of higher frequency oscillations increases, perhaps indicating a relative increase in the numbers and intensity of resonant oscillation of small bubbles.

Fig. 11 shows the AE total power as a function of aeration rate for sensor 9 (the uppermost accelerometer attached 3 m above the discharge nozzle of the downcomer). The trend in total AE power is the reverse of that for sensor 8, with total power monotonically decreasing as aeration rate is increased. It is hypothesised that this decrease in total AE power with aeration rate may be due to movement of the induction trumpet away from the sensor further towards the discharge of the downcomer. Fig. 11 also shows that the AE spectra for the accelerometer mounted highest on the downcomer are highly repeatable.

Fig. 12 shows the AE power spectrum for sensor 9 as a function of aeration rate. Again there are very strong spectral features, highly varying in intensity with aeration rate. In this case the features at ~3 and 5 kHz are more dominant, perhaps indicating that relatively more larger bubbles are present at this physical position in the downcomer (closer to the induction trumpet). The AE spectrum associated with a closed downcomer valve (no slurry or air) shows that most of the spectral features associated with accelerometers mounted on the surface of a downcomer are largely due to the air and slurry within. However the frequency dependent behaviour of the spectra with aeration rate is non-monotonic, with an initially large response at low cell aeration rates decreasing up till ~800 $m^3 h^{-1}$ and then increasing again above ~5 kHz for higher aeration rates. In fact there are differences in the behaviour with aeration rate and shape of AE power spectra measured by each of the four accelerometers mounted along the downcomer. This may be related to different AE source characteristics for the plunging jet, mixing and pipe flow zones of the downcomer (see Fig. 5).

Fig. 13 shows the AE spectral response of sensor 1, a hydrophone positioned above the J-cell diffuser and nominally in the froth zone. There is clearly a reasonably strong low frequency response

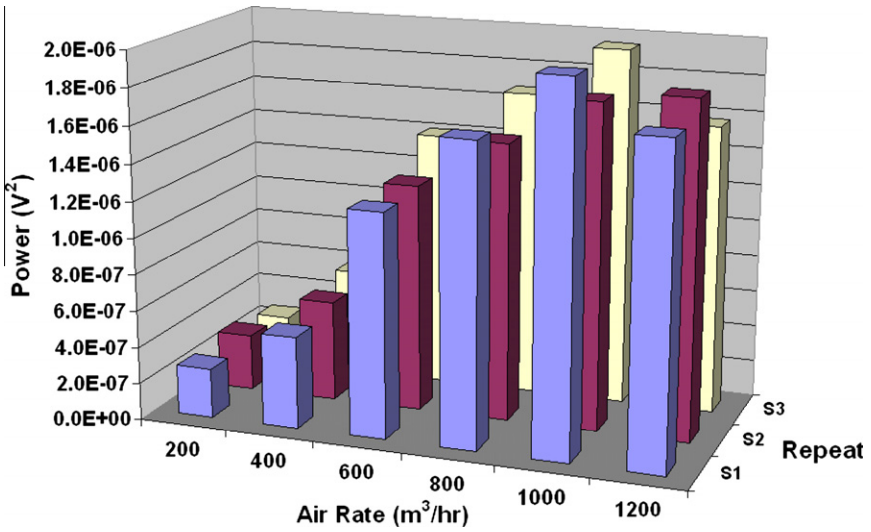

Fig. 9. Total AE power for sensor 8 with variation of air addition rate ($m^3\ h^{-1}$).

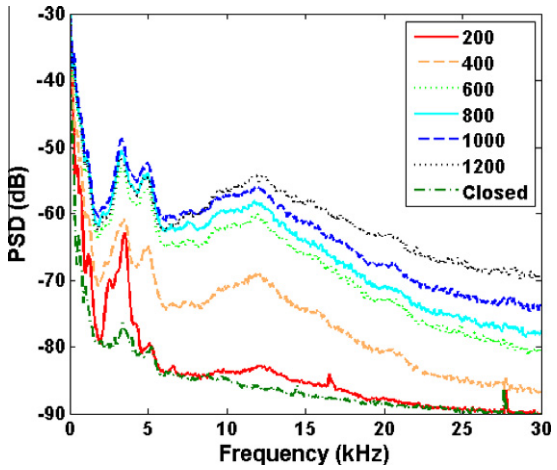

Fig. 10. AE power spectra for sensor 8 (accelerometer mounted near nozzle of downcomer) with variation of J-cell total air addition rate ($m^3\ h^{-1}$). PSD parameters: 2^{12} FFT points, 2^{11} overlap points, Hanning windowing.

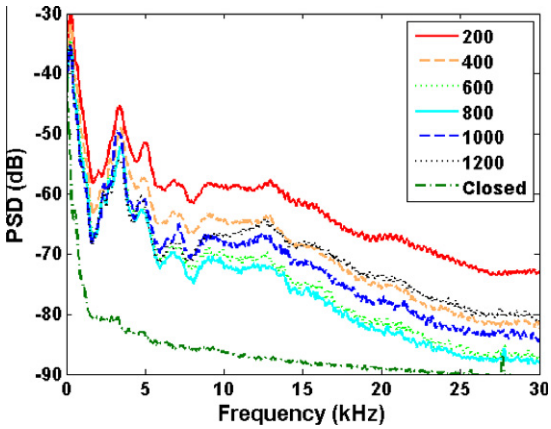

Fig. 12. AE spectra for sensor 9 (accelerometer mounted 3 m above bottom of downcomer) with variation of J-cell total air addition rate ($m^3\ h^{-1}$). PSD parameters: 2^{12} FFT points, 2^{11} overlap points, Hanning windowing.

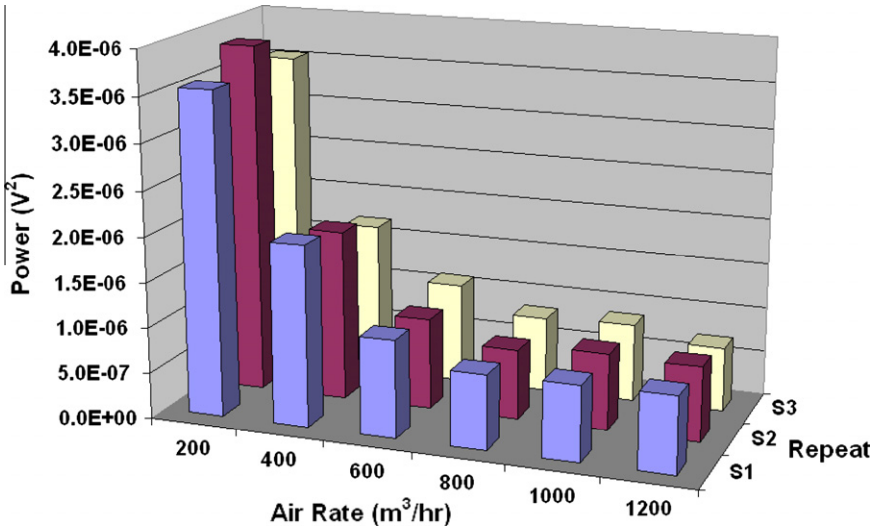

Fig. 11. Total AE power for sensor 9 with variation of air addition rate ($m^3\ h^{-1}$).

out to ~15 kHz, increasing with aeration rate. On this basis it appears that passive AE is detectable in the J-cell froth, for a hydrophone positioned close to the downcomer. A reasonably strong AE response was also logged from hydrophone S3, positioned in the pulp near the air diffuser around the downcomer, but the trends with aeration rate were not as strong (not shown here). There are AE responses from the other two hydrophones but they are not as strong or as variable with aeration rate. Hence most of the bubble-related acoustic activity appears to be restricted to the region near the downcomer. The AE response from accelerometers mounted on the inside of the tank walls was found to be minimal in this study.

4.3.3. Reagent addition rate

A series of tests were performed with variation of frother addition rate (5, 7, and 9 l h^{-1}). In this case the frother level was allowed to adjust for ~30 min before AE measurements were taken. Fig. 14 shows the AE power spectrum as a function of frother addition rate for sensor 7 (accelerometer 1 m above the downcomer discharge orifice). There is a small but significant decrease in passive AE within the downcomer with increasing frother addition, particularly at frequencies above ~1 kHz. However, the addition of frother should result in an increase in the number of bubbles. It is hypothesised that this effect may be due to a change in the surface properties of the bubbles (surface tension), perhaps making them less oscillatory or perhaps due to increased acoustic scattering and damping by the additional bubbles. A comparison of Figs. 10 and 14 reveals that the ~12 kHz passive AE spectral peak detected by the accelerometer mounted near the nozzle of the downcomer (S8) is present at ~9.5 kHz for the accelerometer mounted 1 m higher (S7). An interpretation of this result would require detailed knowledge of the slurry pressure distribution within the downcomer. Certainly it is too large a change to be explained in terms of a 1 m difference in slurry hydrostatic head pressure affecting both the resonance frequency of a bubble of a particular size (see Fig. 1) and the actual equilibrium size of the bubble itself as may be modelled via Boyle's Law.

A series of AE monitoring tests were also performed with variation of collector addition rate (150, 180, and 220 l h^{-1}). The power spectra for sensor 7 associated with these tests (not shown here) reveal a small decrease in passive AE power above ~10 kHz with increasing collector addition rate. This may be due to a change in the surface chemistry of the bubbles in the downcomer, rendering them more like solid bodies. Other possibilities are damping of AE in the downcomer due to increased solids loading on bubbles or increased slurry attenuation of AE due to the addition of collector.

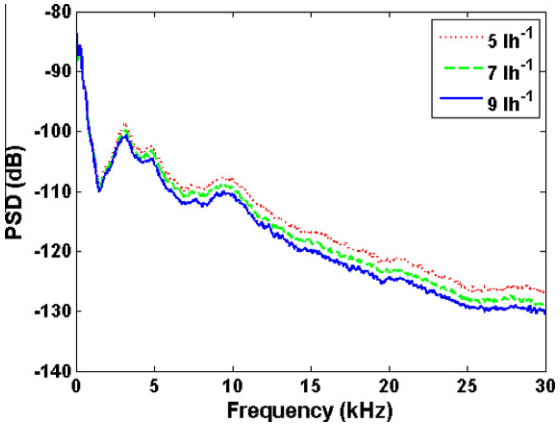

Fig. 14. AE spectra for sensor 7 (second lowest accelerometer on downcomer) with variation of frother addition rate (l h^{-1}). PSD parameters: 2^{12} FFT points, 2^{11} overlap points, Hanning windowing.

Fig. 15 shows the AE power spectrum as a function of frother addition rate for sensor 3 (lower hydrophone in pulp near the diffuser). The total power is consistently largest for the 7 l h^{-1} frother addition rate. However, the spectral response in the range ~5–15 kHz (which may be related to individual bubble oscillations in the pulp near this sensor) is actually lowest for the 7 l h^{-1} frother addition rate. The total power is actually dominated by components at the very lowest frequencies. Spectral features in the range ~5–15 kHz associated with the 9 l h^{-1} frother addition rate are actually highly variable, perhaps indicating instability in bubble population numbers and size distribution in these conditions. However, Fig. 15 clearly shows spectral features in the frequency range ~5–15 kHz that may be bubble resonance related.

4.3.4. Plant solids feed rate variation

A series of passive AE monitoring tests were conducted with variation of the plant total solids feed rate. This was done in order to investigate the relationship between Jameson cell feed solids addition rate and passive acoustic response. The hypothesis is that variation in the coal washery total solids feed rate is reflected by a corresponding change in the solids feed rate to the particular Jameson cell (and hence downcomer) being monitored in the fines circuit. Fig. 16 shows the AE power spectrum (PSD) for sensor 8 (the accelerometer nearest the discharge nozzle of the downcomer) as a function of plant total solids feed rate. The aeration rate was constant at 600 m^3 h^{-1} and J-cell volumetric feed rate steady

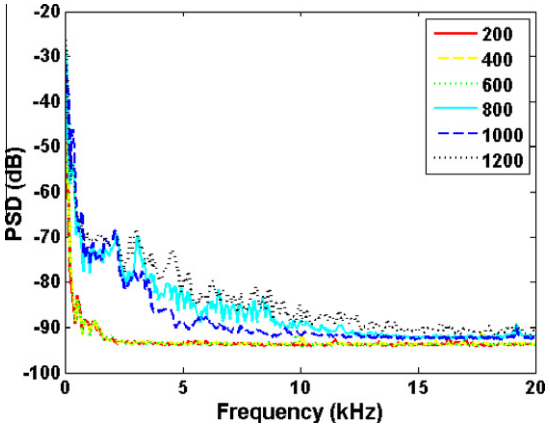

Fig. 13. AE spectra for sensor 1 (hydrophone mounted in froth above diffuser) with variation of air addition rate (m^3 h^{-1}). PSD parameters: 2^{12} FFT points, 2^{11} overlap points, Hanning windowing.

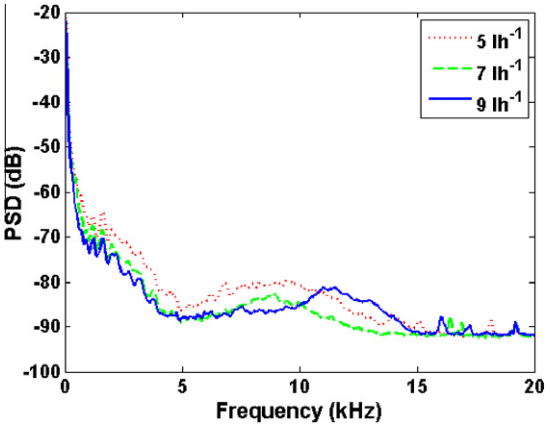

Fig. 15. AE spectra for sensor 3 (lower hydrophone in pulp near the diffuser) with variation of frother addition rate (l h^{-1}). PSD parameters: 2^{12} FFT points, 2^{11} overlap points, Hanning windowing.

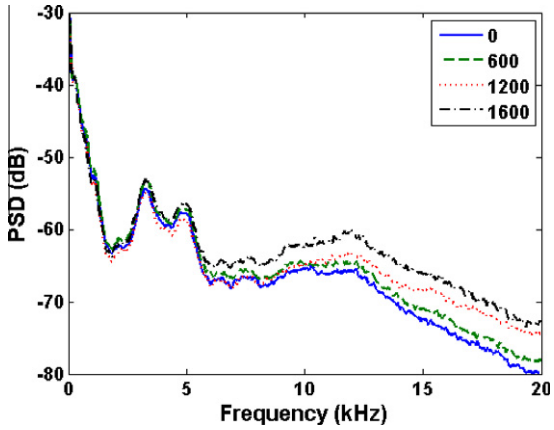

Fig. 16. AE power spectra for sensor 8 (accelerometer mounted near nozzle of downcomer) with variation of total plant solids feed rate (th^{-1}). PSD parameters: 2^{12} FFT points, 2^{11} overlap points, Hanning windowing.

for all of these experiments. Included in this plot is a spectrum associated with a period of nil solids feed rate to the Jameson cell (a feed slurry consisting of process water and reagents), which was identified from plant data as a period with negligible circuit product conveyor belt weightometer reading.

Fig. 16 shows a substantial increase in AE power above ~5 kHz as the total plant solids feed rate increases. A possible explanation is that more free and/or bubble attached solids particles inside the downcomer due to the increase in J-cell solids feed rate may generate more AE by impact on the inside of the downcomer wall. Alternatively, an increase in the solids content of the J-cell feed slurry may result in a decrease in the attenuation of AE generated within the downcomer.

An important effect shown in Fig. 16 is a small but detectable decrease of ~280 Hz in the peak AE frequency near ~12 kHz with increasing total plant solids feed rate. There is no apparent shift in the frequency of the spectral peaks at ~3 and 5 kHz with solids loading. If the frequencies of the ~9–12 kHz spectral features are interpreted in terms of the developed theory of bubble fundamental resonant oscillation frequency and attached solids mass for a distribution of bubble sizes and solids loadings (see Eqs. (2) and (5)), the shift in resonance frequency for the ~12 kHz spectral peak with addition of solids to the feed corresponds to a loading of ~540 μm diameter bubbles with ~0.04 μg of attached solids at full plant solids feed rate (~1600 th^{-1}). This is about 80% of the maximum possible monolayer solids loading for a bubble of this size. On the basis of these results, it appears that it is possible to use passive AE detected by an accelerometer mounted on the external surface of a J-cell downcomer near the discharge to predict some information on the locally dominant pulp bubble size and solids loading just prior to exit of the slurry into the riser section. However, it is not clear purely on the basis of this analysis how to predict the relative numbers of bubbles of a particular size or loading or the total numbers of bubbles and mass of attached solids. Both modelling based on passive AE (Manasseh et al., 2001) and acoustic velocity measurement by active AE (Leighton, 1994; Vanegas and Holtham, 2010) may be used to estimate the local void fraction.

5. Conclusion

A passive AE monitoring system has been used to investigate the natural acoustic emission signature of a Jameson flotation cell in an Australian coal washery. A combination of hydrophones and accelerometers were used to monitor passive AE in the downcomer, riser section pulp and froth zones of the cell. The study found that strong passive AE can be detected in the Jameson cell by accelerometers mounted on the outside of a downcomer and hydrophones positioned nearby in both the riser section pulp and froth zones. These sensors are shown to detect passive AE signatures which significantly vary with aeration and feed solids rate, and more modestly with frother and collector addition rates. Contact AE monitoring by accelerometers mounted on the outside of a downcomer is highly sensitive to aeration rate. It is reasonably hypothesised that the accelerometer AE signals are due to bubble oscillations and slurry flow inside the downcomer local to the sensor, filtered by transmission through the downcomer.

AE signals from downcomer mounted accelerometers contain spectral features that can be interpreted in terms of Minnaert bubble resonance theory for bubbles with attached solids. The ~9–12 kHz spectral peaks evident in the downcomer accelerometer Fourier power spectra are used to infer ~540–710 μm diameter locally dominant bubble sizes near the downcomer discharge orifice. The change in peak frequency between bubbles with normal solids loading and in the case of nil solids feed is used to estimate ~0.04 μg of attached solids mass per bubble at full plant solids feed rate for the most dominant bubble size (~540 μm diameter). This is about 80% of the maximum possible monolayer solids loading for a bubble of this size. The comparison of unloaded to solids loaded AE spectra, for downcomer mounted accelerometers, could be used for on-line monitoring of J-cell downcomer bubble size and attached solids mass loading in both metalliferous mineral processing plants and coal washeries. It should be noted that no attempt has been made to account for any bubble swarm group effects in this analysis.

The use of passive AE monitoring appears to be particularly effective in estimating local bubble size and solids loading characteristics for the case of accelerometers mounted on the outside of a downcomer. This is probably both because the downcomer is the region of bubble generation and the jet flow within is very energetic in comparison to the flow in the riser region, providing additional turbulent energy for sustained bubble resonant oscillations. More generally, passive AE monitoring by hydrophones and accelerometers is a promising approach in both pulp and froth for flotation cell performance on-line monitoring. Further results from ACARP project C17042 will be used in a later paper to demonstrate the applicability of the passive AE monitoring method to Microcel column flotation performance monitoring. Active AE monitoring methods are expected to be particularly useful for monitoring bubble size and attached mass population characteristics and in flotation cell pulp riser regions with a low level of natural emissions.

Acknowledgements

The authors gratefully acknowledge the financial assistance of the Australian Coal Association Research Program for partial funding of Project C17042 under which some of this work was performed. The staff of the Australian coal washery involved in the Jameson cell AE monitoring experimental campaign are also thanked for their diligent assistance.

References

Al-Masry, W.A., Ali, E.M., Aqeel, Y.M., 2005. Determination of bubble characteristics in bubble columns using statistical analysis of acoustic sound measurements. Chemical Engineering Research and Design 83 (A10), 1196–1207.

Ata, S., Jameson, G., 2005. The formation of bubble clusters in flotation cells. International Journal of Mineral Processing 76, 123–139.

Bournival, G., Ata, S., 2010. Packing of particles on the surface of bubbles. Minerals Engineering 23, 111–116.

Boyd, J.W.R., Varley, J., 2001. The uses of passive measurement of acoustic emissions from chemical engineering processes. Chemical Engineering Science 56, 1749–1767.

Bruniges, R., Millen, M., Rainey, S., Sharp, V., Spencer, S.J., Stevens, R., Williams, A., 2008. Development of a commercial prototype on-line adverse operation condition alarm system for dense medium cyclones. In: Mathewson, D. (Ed.), Proceedings of the 12th Australian Coal Preparation Congress and Exhibition. pp. 96-108.

Campbell, J.J., Holmes, R.J., Spencer, S.J., Phillips, P.L., Barker, D.G., Davey, K.J., 2006. An on-line surface vibration monitoring system for AG/SAG mills. In: Onal, G. et al. (Eds.), Proceedings of the XXIII International Mineral Processing Congress. Turkish Mining Development Foundation, Istanbul, pp. 1747–1752.

Church, C.C., 1995. The effects of an elastic solid surface layer on the radial pulsations of gas bubbles. Journal of the Acoustical Society of America 97 (3), 1510–1521.

Holtham, P., Power, A., 2002. Optimisation of fine coal flotation. ACARP Project C7042 Report, Australian Coal Association Research Program.

Hou, R., Hunt, A., Williams, R.A., 1998. Acoustic monitoring of hydrocyclone performance. Minerals Engineering 11, 1047–1059.

Hu, S., Firth, B., 2010. Plant-based trials of monitoring of coal flotation systems using electrical impedance spectrum technique. In: Holmes, R.J. et al. (Eds.), Proceedings of the XXV International Mineral Processing Congress. AUSIMM, Melbourne, pp. 1991–2001.

Kihm, K.D., Deignan, P., 1995. Dynamic surface tension of coal-water slurry fuels. Fuel 74 (2), 295–300.

Kolaini, A.R., Goumilevski, A.G., 1997. Acoustic characterization of an adult bubble injected into a fully developed turbulent flow field. Journal of the Acoustical Society of America 101 (1), 218–226.

Leighton, T.G., 1994. The Acoustic Bubble. Academic Press, New York.

Leighton, T.G., Phelps, A.D., Ramble, D.G., Sharpe, D.A., 1996. Comparison of the abilities of eight acoustic techniques to detect and size a single bubble. Ultrasonics 34 (6), 661–667.

Leighton, T.G., Ramble, D.G., Phelps, A.D., 1997. The detection of tethered and rising bubbles using multiple acoustic techniques. Journal of the Acoustical Society of America 101 (5), 2626–2635.

Manasseh, R., Ooi, A., 2009. Frequencies of acoustically interacting bubbles. Bubble Science, Engineering and Technology 1, 58–74.

Manasseh, R., LaFontaine, R.F., Davy, J., Shepherd, I., Zhu, Y.-G., 2001. Passive acoustic bubble sizing in sparged systems. Experiments in Fluids 30, 672–682.

Neese, T., Tiefel, H., Kaniut, P., 2006. Volume split control in hydrocyclone separation. In: Onal, G. et al. (Eds.), Proceedings of the XXIII International Mineral Processing Congress. Turkish Mining Development Foundation, Istanbul, pp. 1771–1776.

Omota, F., Dimian, A.C., Bliek, A., 2006. Adhesion of solid particles to gas bubbles. part 1: modelling. Chemical Engineering Science 61, 823–834.

Pyecha, J., Lacouture, B., Sims, S., Hope, G., Stradling, A., 2006. Evaluation of a microcel TM sparger in the red dog column flotation cells. Minerals Engineering 19, 748–757.

Spencer, S.J., Liu, Y., Sharp, V., Bruniges, R., 2006a. Acoustic emission monitoring of dense medium cyclones. In: Onal, G. et al. (Eds.), Proceedings of the XXIII International Mineral Processing Congress. Turkish Mining Development Foundation, Istanbul, pp. 1765–1770.

Spencer, S.J., Sharp, V., Campbell, J.J., Holmes, R.J., Rowlands, T., Barker, D.G., Davey, K.J., Phillips, P.L., 2006b. Prediction of AG/SAG mill variables from surface vibrations. In: Onal, G. et al. (Eds.), Proceedings of the XXIII International Mineral Processing Congress. Turkish Mining Development Foundation, Istanbul, pp. 44–49.

Spencer, S.J., Bruniges, R., Williams, A., Sharp, V., Rainey, S., Roberts, G., Stevens, R., Millen, M., 2008. Acoustic emission soft-sensor alarm system for dense medium cyclones. ACARP Project C16045 Report, Australian Coal Association Research Program.

Spencer, S.J., Bruniges, R., Sharp, V., Catanzano, V., Roberts, G., Bruckard, W.J., Davey, K., 2010. Acoustic emission monitoring of froth flotation. In: Holmes, R.J. et al. (Eds.), Proceedings of the XXV International Mineral Processing Congress. AUSIMM, Melbourne, pp. 3489–3500.

Vanegas, C., Holtham, P., 2008. On-line froth acoustic emission measurements on industrial sites. Minerals Engineering 21, 883–888.

Vanegas, C., Holtham, P., 2010. Possibilities for flotation acoustics monitoring – a review. In: Holmes, R.J. et al. (Eds.), Proceedings of the XXV International Mineral Processing Congress. AUSIMM, Melbourne, pp. 2457–2470.

Young, M.F., Barnes, K.E., Anderson, G.S., Pease, J.D., 2006. Jameson Cell: The "comeback" in base metals applications using improved design and flow sheets. In: Proceedings of the 38th Annual Meeting of Canadian Mineral Processors. Ottawa, pp. 311-332.

Zhang, W., Spencer, S.J., Coghill, P., 2012. An acoustic technique for measurement of bubble solids mass loading (a) fundamental study of a single bubble. Minerals Engineering, accepted for publication.